BELLE-CONF-0567
EPS05-542

Measurement of Exclusive $B \to X_u \ell\nu$ Decays with $D^{(*)}\ell\nu$ Decay Tagging

K. Abe,[9] K. Abe,[47] I. Adachi,[9] H. Aihara,[49] K. Aoki,[23] K. Arinstein,[2] Y. Asano,[54] T. Aso,[53] V. Aulchenko,[2] T. Aushev,[13] T. Aziz,[45] S. Bahinipati,[5] A. M. Bakich,[44] V. Balagura,[13] Y. Ban,[36] S. Banerjee,[45] E. Barberio,[22] M. Barbero,[8] A. Bay,[19] I. Bedny,[2] U. Bitenc,[14] I. Bizjak,[14] S. Blyth,[25] A. Bondar,[2] A. Bozek,[29] M. Bračko,[9,21,14] J. Brodzicka,[29] T. E. Browder,[8] M.-C. Chang,[48] P. Chang,[28] Y. Chao,[28] A. Chen,[25] K.-F. Chen,[28] W. T. Chen,[25] B. G. Cheon,[4] C.-C. Chiang,[28] R. Chistov,[13] S.-K. Choi,[7] Y. Choi,[43] Y. K. Choi,[43] A. Chuvikov,[37] S. Cole,[44] J. Dalseno,[22] M. Danilov,[13] M. Dash,[56] L. Y. Dong,[11] R. Dowd,[22] J. Dragic,[9] A. Drutskoy,[5] S. Eidelman,[2] Y. Enari,[23] D. Epifanov,[2] F. Fang,[8] S. Fratina,[14] H. Fujii,[9] N. Gabyshev,[2] A. Garmash,[37] T. Gershon,[9] A. Go,[25] G. Gokhroo,[45] P. Goldenzweig,[5] B. Golob,[20,14] A. Gorišek,[14] M. Grosse Perdekamp,[38] H. Guler,[8] R. Guo,[26] J. Haba,[9] K. Hara,[9] T. Hara,[34] Y. Hasegawa,[42] N. C. Hastings,[49] K. Hasuko,[38] K. Hayasaka,[23] H. Hayashii,[24] M. Hazumi,[9] T. Higuchi,[9] L. Hinz,[19] T. Hojo,[34] T. Hokuue,[23] Y. Hoshi,[47] K. Hoshina,[52] S. Hou,[25] W.-S. Hou,[28] Y. B. Hsiung,[28] Y. Igarashi,[9] T. Iijima,[23] K. Ikado,[23] A. Imoto,[24] K. Inami,[23] A. Ishikawa,[9] H. Ishino,[50] K. Itoh,[49] R. Itoh,[9] M. Iwasaki,[49] Y. Iwasaki,[9] C. Jacoby,[19] C.-M. Jen,[28] R. Kagan,[13] H. Kakuno,[49] J. H. Kang,[57] J. S. Kang,[16] P. Kapusta,[29] S. U. Kataoka,[24] N. Katayama,[9] H. Kawai,[3] N. Kawamura,[1] T. Kawasaki,[31] S. Kazi,[5] N. Kent,[8] H. R. Khan,[50] A. Kibayashi,[50] H. Kichimi,[9] H. J. Kim,[18] H. O. Kim,[43] J. H. Kim,[43] S. K. Kim,[41] S. M. Kim,[43] T. H. Kim,[57] K. Kinoshita,[5] N. Kishimoto,[23] S. Korpar,[21,14] Y. Kozakai,[23] P. Križan,[20,14] P. Krokovny,[9] T. Kubota,[23] R. Kulasiri,[5] C. C. Kuo,[25] H. Kurashiro,[50] E. Kurihara,[3] A. Kusaka,[49] A. Kuzmin,[2] Y.-J. Kwon,[57] J. S. Lange,[6] G. Leder,[12] S. E. Lee,[41] Y.-J. Lee,[28] T. Lesiak,[29] J. Li,[40] A. Limosani,[9] S.-W. Lin,[28] D. Liventsev,[13] J. MacNaughton,[12] G. Majumder,[45] F. Mandl,[12] D. Marlow,[37] H. Matsumoto,[31] T. Matsumoto,[51] A. Matyja,[29] Y. Mikami,[48] W. Mitaroff,[12] K. Miyabayashi,[24] H. Miyake,[34] H. Miyata,[31] Y. Miyazaki,[23] R. Mizuk,[13] D. Mohapatra,[56] G. R. Moloney,[22] T. Mori,[50] A. Murakami,[39] T. Nagamine,[48] Y. Nagasaka,[10] T. Nakagawa,[51] I. Nakamura,[9] E. Nakano,[33] M. Nakao,[9] H. Nakazawa,[9] Z. Natkaniec,[29] K. Neichi,[47] S. Nishida,[9] O. Nitoh,[52] S. Noguchi,[24] T. Nozaki,[9] A. Ogawa,[38] S. Ogawa,[46] T. Ohshima,[23] T. Okabe,[23] S. Okuno,[15] S. L. Olsen,[8] Y. Onuki,[31] W. Ostrowicz,[29] H. Ozaki,[9] P. Pakhlov,[13] H. Palka,[29] C. W. Park,[43] H. Park,[18] K. S. Park,[43] N. Parslow,[44] L. S. Peak,[44] M. Pernicka,[12] R. Pestotnik,[14] M. Peters,[8] L. E. Piilonen,[56] A. Poluektov,[2] F. J. Ronga,[9] N. Root,[2] M. Rozanska,[29] H. Sahoo,[8] M. Saigo,[48] S. Saitoh,[9] Y. Sakai,[9] H. Sakamoto,[17] H. Sakaue,[33] T. R. Sarangi,[9] M. Satapathy,[55] N. Sato,[23] N. Satoyama,[42] T. Schietinger,[19] O. Schneider,[19] P. Schönmeier,[48] J. Schümann,[28] C. Schwanda,[12] A. J. Schwartz,[5] T. Seki,[51] K. Senyo,[23] R. Seuster,[8] M. E. Sevior,[22] T. Shibata,[31] H. Shibuya,[46] J.-G. Shiu,[28] B. Shwartz,[2] V. Sidorov,[2] J. B. Singh,[35] A. Somov,[5] N. Soni,[35] R. Stamen,[9] S. Stanič,[32] M. Starič,[14] A. Sugiyama,[39] K. Sumisawa,[9] T. Sumiyoshi,[51] S. Suzuki,[39] S. Y. Suzuki,[9] O. Tajima,[9] N. Takada,[42] F. Takasaki,[9] K. Tamai,[9] N. Tamura,[31] K. Tanabe,[49] M. Tanaka,[9] G. N. Taylor,[22] Y. Teramoto,[33] X. C. Tian,[36] K. Trabelsi,[8]

Y. F. Tse,[22] T. Tsuboyama,[9] T. Tsukamoto,[9] K. Uchida,[8] Y. Uchida,[9] S. Uehara,[9] T. Uglov,[13] K. Ueno,[28] Y. Unno,[9] S. Uno,[9] P. Urquijo,[22] Y. Ushiroda,[9] G. Varner,[8] K. E. Varvell,[44] S. Villa,[19] C. C. Wang,[28] C. H. Wang,[27] M.-Z. Wang,[28] M. Watanabe,[31] Y. Watanabe,[50] L. Widhalm,[12] C.-H. Wu,[28] Q. L. Xie,[11] B. D. Yabsley,[56] A. Yamaguchi,[48] H. Yamamoto,[48] S. Yamamoto,[51] Y. Yamashita,[30] M. Yamauchi,[9] Heyoung Yang,[41] J. Ying,[36] S. Yoshino,[23] Y. Yuan,[11] Y. Yusa,[48] H. Yuta,[1] S. L. Zang,[11] C. C. Zhang,[11] J. Zhang,[9] L. M. Zhang,[40] Z. P. Zhang,[40] V. Zhilich,[2] T. Ziegler,[37] and D. Zürcher[19]

(The Belle Collaboration)

[1]*Aomori University, Aomori*
[2]*Budker Institute of Nuclear Physics, Novosibirsk*
[3]*Chiba University, Chiba*
[4]*Chonnam National University, Kwangju*
[5]*University of Cincinnati, Cincinnati, Ohio 45221*
[6]*University of Frankfurt, Frankfurt*
[7]*Gyeongsang National University, Chinju*
[8]*University of Hawaii, Honolulu, Hawaii 96822*
[9]*High Energy Accelerator Research Organization (KEK), Tsukuba*
[10]*Hiroshima Institute of Technology, Hiroshima*
[11]*Institute of High Energy Physics, Chinese Academy of Sciences, Beijing*
[12]*Institute of High Energy Physics, Vienna*
[13]*Institute for Theoretical and Experimental Physics, Moscow*
[14]*J. Stefan Institute, Ljubljana*
[15]*Kanagawa University, Yokohama*
[16]*Korea University, Seoul*
[17]*Kyoto University, Kyoto*
[18]*Kyungpook National University, Taegu*
[19]*Swiss Federal Institute of Technology of Lausanne, EPFL, Lausanne*
[20]*University of Ljubljana, Ljubljana*
[21]*University of Maribor, Maribor*
[22]*University of Melbourne, Victoria*
[23]*Nagoya University, Nagoya*
[24]*Nara Women's University, Nara*
[25]*National Central University, Chung-li*
[26]*National Kaohsiung Normal University, Kaohsiung*
[27]*National United University, Miao Li*
[28]*Department of Physics, National Taiwan University, Taipei*
[29]*H. Niewodniczanski Institute of Nuclear Physics, Krakow*
[30]*Nippon Dental University, Niigata*
[31]*Niigata University, Niigata*
[32]*Nova Gorica Polytechnic, Nova Gorica*
[33]*Osaka City University, Osaka*
[34]*Osaka University, Osaka*
[35]*Panjab University, Chandigarh*
[36]*Peking University, Beijing*
[37]*Princeton University, Princeton, New Jersey 08544*

[38]RIKEN BNL Research Center, Upton, New York 11973
[39]Saga University, Saga
[40]University of Science and Technology of China, Hefei
[41]Seoul National University, Seoul
[42]Shinshu University, Nagano
[43]Sungkyunkwan University, Suwon
[44]University of Sydney, Sydney NSW
[45]Tata Institute of Fundamental Research, Bombay
[46]Toho University, Funabashi
[47]Tohoku Gakuin University, Tagajo
[48]Tohoku University, Sendai
[49]Department of Physics, University of Tokyo, Tokyo
[50]Tokyo Institute of Technology, Tokyo
[51]Tokyo Metropolitan University, Tokyo
[52]Tokyo University of Agriculture and Technology, Tokyo
[53]Toyama National College of Maritime Technology, Toyama
[54]University of Tsukuba, Tsukuba
[55]Utkal University, Bhubaneswer
[56]Virginia Polytechnic Institute and State University, Blacksburg, Virginia 24061
[57]Yonsei University, Seoul

Abstract

We report a measurement of the charmless semileptonic decays $B^0 \to \pi^-/\rho^-\ell^+\nu$ and $B^+ \to \pi^0/\rho^0\ell^+\nu$, based on 253 fb^{-1} of data collected with the Belle detector at the KEKB e^+e^- asymmetric collider. In this analysis, the accompanying B meson is reconstructed in the semileptonic mode $B \to D^{(*)}\ell\nu$, enabling detection of the signal modes with high purity. We measure the branching fractions $\mathcal{B}(B^0 \to \pi^-\ell^+\nu) = (1.48 \pm 0.20 \pm 0.16 \pm 0.04) \times 10^{-4}$, $\mathcal{B}(B^0 \to \rho^-\ell^+\nu) = (2.07 \pm 0.47 \pm 0.25 \pm 0.14) \times 10^{-4}$, $\mathcal{B}(B^+ \to \pi^0\ell^+\nu) = (0.76 \pm 0.13 \pm 0.08 \pm 0.04) \times 10^{-4}$ and $\mathcal{B}(B^+ \to \rho^0\ell^+\nu) = (1.39 \pm 0.23 \pm 0.17 \pm 0.03) \times 10^{-4}$, where the errors are statistical, experimental systematic, and systematic due to form-factor uncertainties, respectively. For each mode we also present the partial branching fractions in three q^2 intervals; $q^2 < 8$, $8 \leq q^2 < 16$, and $q^2 \geq 16\,\mathrm{GeV}^2/c^2$. Based on these results, the magnitude of the Cabibbo-Kobayashi-Maskawa matrix element V_{ub} is extracted. All of the presented results are preliminary.

PACS numbers: 12.15.Hh, 12.38.Gc, 13.25.Hw

INTRODUCTION

Exclusive $B \to X_u \ell\nu$ decays proceed dominantly via a $b \to uW^-$ tree process and can be used to determine $|V_{ub}|$, one of the smallest and least known elements of the Cabibbo-Kobayashi-Maskawa matrix [1]. A major theoretical uncertainty stems from the specification of form-factors (FF) involved in the decays. The recent release of preliminary results from unquenched Lattice QCD(LQCD) calculations of FFs [2, 3] has made possible the model-independent determination of $|V_{ub}|$. Since LQCD results are available only in the high q^2 region ($\geq 16\,\mathrm{GeV}^2/c^2$), a clean measurement of the partial $B \to \pi\ell\nu$ branching fraction in the same high q^2 region is essential.

There have been several measurements in the past by CLEO, BaBar and Belle for the $B \to \pi\ell\nu$, $\rho\ell\nu$, $\eta\ell\nu$ and $\omega\ell\nu$ modes. The analyses in [4, 5, 6, 7, 8, 9] utilize the method, originally developed by CLEO, where the B decays are reconstructed by inferring the undetected neutrino momentum from missing energy and momentum ("ν-reconstruction method") [4]. In the B-factory era, we may straightforwardly improve the statistical precision by simply applying the ν-reconstruction method. However, the systematic uncertainty limits the measurement because of a poor signal-to-noise ratio.

The Belle collaboration has previously presented measurements of $B^0 \to \pi^-/\rho^-\ell^+\nu$ via $D^{(*)}\ell\nu$ decay tagging based on 140 fb^{-1} data [10]. The work demonstrated that the method allows one to detect the signal with high purity and is a promising approach to yield the best overall precision from the large data sample being accumulated by B-factories over the next few years. The BaBar collaboration also presented measurements of exclusive $B \to X_u\ell\nu$ decays, both with $D^{(*)}\ell\nu$ decay tagging [11, 12] and with hadronic decay tagging [13].

In this paper we present measurements of $B^0 \to \pi^-/\rho^-\ell^+\nu$ and $B^+ \to \pi^0/\rho^0\ell^+\nu$ decays using $D^{(*)}\ell\nu$ decay tagging and based on 253 fb^{-1} data. In comparison with the previous measurement [10], the analysis has been extended to higher integrated luminosity and to the additional modes $B^+ \to \pi^0/\rho^0\ell^+\nu$. The analysis technique is nearly identical to the previous one; we reconstruct the entire decay chain from the $\Upsilon(4S)$, $\Upsilon(4S) \to B_{sig}B_{tag}$, $B_{sig} \to \pi/\rho\ell\nu$ and $B_{tag} \to D^{(*)}\ell\bar{\nu}$ with several $D^{(*)}$ sub-modes. The back-to-back correlation of the two B mesons in the $\Upsilon(4S)$ rest frame allows us to constrain the kinematics of the double semileptonic decay. Inclusion of charge conjugate decays is implied throughout this paper.

DATA SET AND EXPERIMENT

The analysis is based on data recorded with the Belle detector at the asymmetric e^+e^- collider KEKB operating at the center-of-mass (c.m.) energy of the $\Upsilon(4S)$ resonance [14]. The $\Upsilon(4S)$ data set used for this study corresponds to an integrated luminosity of 253 fb^{-1} and contains 275.2×10^6 $B\bar{B}$ events.

The Belle detector is a large-solid-angle magnetic spectrometer that consists of a silicon vertex detector (SVD), a 50-layer central drift chamber (CDC), an array of aerogel threshold Čerenkov counters (ACC), a barrel-like arrangement of time-of-flight scintillation counters (TOF), and an electromagnetic calorimeter comprised of CsI(Tl) crystals (ECL) located inside a super-conducting solenoid coil that provides a 1.5 T magnetic field. An iron flux-return located outside of the coil is instrumented to detect K_L^0 mesons and to identify muons (KLM). The detector is described in detail elsewhere [15]. Two inner detector configurations were used. A 2.0 cm beampipe and a 3-layer silicon vertex detector was used for the first sample of 152 million $B\bar{B}$ pairs, while a 1.5 cm beampipe, a 4-layer silicon detector, and a

small-cell inner drift chamber were used to record the remaining 123 million $B\bar{B}$ pairs[16].

A detailed Monte Carlo (MC) simulation, which fully describes the detector geometry and response and is based on GEANT [17], is applied to estimate the signal detection efficiency and to study the background. To examine the FF dependence, MC samples for the $B \to \pi\ell\nu$ signal decays are generated with different form-factor models; a quark model (ISGW II [18]), light cone sum rules (LCSR; Ball'01 for $\pi\ell\nu$ [19] and Ball'98 for $\rho\ell\nu$ [20]) and quenched lattice QCD (UKQCD [21]). A relativistic quark model (Melikhov [22]) is also used for $\rho\ell\nu$. To model the cross-feed from other $B \to X_u\ell\nu$ decays, MC samples are generated with the ISGW II model for the resonant components and the DeFazio-Neubert model [23] for non-resonant component ($\pi\ell\nu$ and $\rho\ell\nu$ components are excluded in this sample). To model the $B\bar{B}$ and continuum backgrounds, large generic $B\bar{B}$ (based on Evtgen [24]) and $q\bar{q}$ Monte Carlo samples are used.

EVENT RECONSTRUCTION AND SELECTION

Charged particle tracks are reconstructed from hits in the SVD and CDC. They are required to satisfy track quality cuts based on their impact parameters relative to the measured profile of the interaction point (IP profile) of the two beams. Charged kaons are identified by combining information on ionization loss (dE/dx) in the CDC, Čherenkov light yields in the ACC and time-of-flight measured by the TOF system. For the nominal requirement, the kaon identification efficiency is approximately 88% and the rate for misidentification of pions as kaons is about 8%. Hadron tracks that are not identified as kaons are treated as pions. Tracks satisfying the lepton identification criteria, as described later, are removed from consideration.

Neutral pions are reconstructed using γ pairs with an invariant mass between 117 and 150 MeV/c^2. Each γ is required to have a minimum energy deposit of 50 MeV. K^0_S mesons are reconstructed using pairs of charged tracks that have an invariant mass within ± 12 MeV/c^2 of the known K^0_S mass.

Electron identification is based on a combination of dE/dx in CDC, the response of ACC, shower shape in ECL and the ratio of energy deposit in ECL to the momentum measured by the tracking system. Muon identification by KLM is performed by resistive plate counters interleaved in the iron yoke. The lepton identification efficiencies are estimated to be about 90% for both electrons and muons in the momentum region above 1.2 GeV/c. where leptons from prompt B decays dominate. The hadron misidentification rate is measured using reconstructed $K^0_S \to \pi^+\pi^-$ and found to be less than 0.2% for electrons and 1.5% for muons in the same momentum region.

For the reconstruction of $B_{tag} \to D^{(*)}\ell\bar{\nu}$, the lepton candidate is required to have the correct sign charge with respect to the D meson flavor and a laboratory momentum greater than 1.0 GeV/c ($p^{lab}_\ell > 1.0$ GeV/c). The D meson candidates are reconstructed by using 7 decay modes of D^+ – $D^+ \to K^-\pi^+\pi^+$, $K^-\pi^+\pi^+\pi^0$, $K^0_S\pi^+$, $K^0_S\pi^+\pi^0$, $K^0_S\pi^+\pi^+\pi^-$, $K^+K^0_S$, $K^+K^-\pi^+$– and 10 decay modes of D^0 – $D^0 \to K^-\pi^+$, $K^-\pi^+\pi^0$, $K^-\pi^+\pi^+\pi^-$, $K^0_S\pi^0$, $K^0_S\pi^+\pi^-$, $K^0_S\pi^+\pi^-\pi^0$, $K^-\pi^+\pi^+\pi^-\pi^0$, K^+K^-, $K^0_SK^+K^-$, $K^0_SK^-\pi^+$. The candidates are required to have an invariant mass m_D within $\pm 2.5\sigma$ (σ is a standard deviation) of the nominal D mass, where the mass resolution σ is dependent on the decay mode. D^* mesons are reconstructed by combining the D meson candidate and a charged or neutral pion, $D^{*+} \to D^0\pi^+$, $D^+\pi^0$ and $D^{*0} \to D^0\pi^0$. Each D^* candidate is required to have a mass difference $\Delta m = m_{\bar{D}\pi} - m_{\bar{D}}$ within $\pm 2.5\sigma$ of the nominal values.

For the reconstruction of $B_{sig} \to X_u \ell \nu$, the lepton candidate is required to have the right sign charge with respect to the X_u system and $p_\ell^{lab} > 0.8$ GeV/c. The X_u system may consist of one pion or two pions ($N_{\pi^+} = 1$ or $N_{\pi^+} = N_{\pi^0} = 1$ for a $\bar{B}^0$ tag and $N_{\pi^0} = 1$ or $N_{\pi^+} = N_{\pi^-} = 1$ for a B^- tag). The event is required to have no additional charged tracks or π^0 candidates. We also require that the residual energy from neutral clusters be less than 0.15 GeV ($E_{neut} < 0.15\,\mathrm{GeV}$). The two leptons on the tag and the signal sides are required to have opposite charge. The loss of signal due to $B^0 - \bar{B}^0$ mixing is estimated by MC simulation.

We then impose a constraint based on the kinematics of the double semileptonic decay in the $\Upsilon(4S)$ rest frame. In the semileptonic decay on each side, $B_{1(2)} \to Y_{1(2)}\nu$ ($Y_1 = D^{(*)}\ell$ and $Y_2 = X_u\ell$), the angle between the $B_{1(2)}$ meson and the detected $Y_{1(2)}$ system $\theta_{B_{1(2)}}$ is calculated from the relation, $p_\nu^2 = (p_B - p_Y)^2 = 0$ and the known P_B (the absolute momentum of the mother B meson). This means that the $B_{1(2)}$ direction is constrained on the surface of a cone defined with the angle $\theta_{B_{1(2)}}$ around the direction of the $Y_{1(2)}$ system, as shown graphically in Figure 1. Then the back-to-back relation of the two B meson directions implies that the real B direction is on the cross lines of the two cones when one of the B system is spatially inverted. Denoting θ_{12} the angle between the $D^*\ell$ and the $X_u\ell$ systems, the B directional vector $\vec{n}_B = (x_B, y_B, z_B)$ is given by, $z_B = \cos\theta_{B_1}$, $y_B = (\cos\theta_{B_2} - \cos\theta_{B_2}\cos\theta_{12})/\sin\theta_{12}$, and

$$x_B = \pm\sqrt{1 - \frac{1}{\sin\theta_{12}}(\cos^2\theta_{B_1} + \cos^2\theta_{B_2} - 2\cos\theta_{B_1}\cos\theta_{B_2}\cos\theta_{12})} \qquad (1)$$

with the coordinate definition in Figure 1. If the hypothesis of the double semileptonic decay is correct and all the decay products are detected except for the two neutrinos, x_B^2 must range from 0 to 1. Events passing a rather loose cut $x_B^2 > -2.0$ are used for signal extraction at a later stage of the analysis.

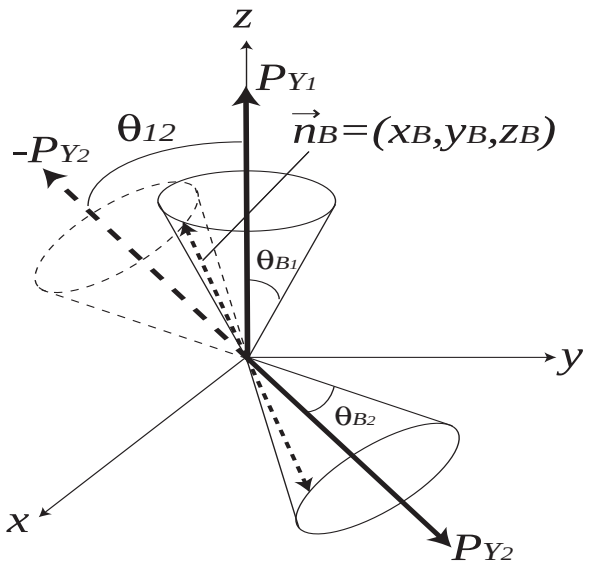

FIG. 1: Kinematics of the double semileptonic decay.

Since Eq. 1 has two solutions and the direction of the B meson is not uniquely determined, we calculate, q^2 as $q^2 = (E^*_{beam} - E^*_{X_u})^2 - p^{*}_{X_u}{}^2$, using the beam energy (E^*_{beam}), energy ($E^*_{X_u}$)

and momentum ($p^*_{X_u}$) of the X_u system and neglecting the momentum of the B meson in the c.m. system. The signal Monte Carlo simulation predicts the average q^2 resolution to be approximately $0.75\,\mathrm{GeV}^2/c^2$.

According to Monte Carlo simulations, the major backgrounds originate with $B \to X_c \ell\nu$ and non-signal $B \to X_u \ell\nu$ decays, where some particles escape detection. There are sizable contributions from cross talk between the $\bar{B}^0$ and B^+ tags. The contribution from $q\bar{q}$ processes is found to be negligible.

For events selected as described above, the signal MC simulation indicates that the total detection efficiency (ϵ_{total}), on the average of the electron and muon channels, is 2.00×10^{-3} for $\pi^-\ell^+\nu$ and 7.75×10^{-4} for $\rho^-\ell^+\nu$, 1.49×10^{-3} for $\pi^0\ell^+\nu$ and 1.76×10^{-3} for $\rho^0\ell^+\nu$ assuming the LCSR model. Here, ϵ_{total} is defined with respect to the number of produced $B\bar{B}$ pairs where one B decays into the signal mode, and includes the loss of signal due to $B^0 - \bar{B}^0$ mixing. Because of the relaxed lepton momentum cut ($> 0.8\,\mathrm{GeV}/c$), the variation of efficiency with different FF models is relatively small.

The validity of the method to reconstruct the double semileptonic decay is checked by reconstructing the signal as $B^0_{sig} \to D^{*-}\ell^+\nu$ followed by $D^{*-} \to \bar{D}^0\pi^-, \bar{D}^0 \to K^+\pi^-$, with the same requirement on the tagging side. Figure 2-a) shows the obtained $M_{K\pi\pi}$ distribution and its MC expectation. With the 253 fb^{-1} data sample, 224.7 ± 15.4 decays are clearly identified, while the expectation based on the MC efficiency and the product branching fraction $\mathcal{B}(B^0 \to D^{*-}\ell^+\nu, D^{*-} \to \bar{D}^0\pi^-, \bar{D}^0 \to K^+\pi^-) = (1.38 \pm 0.06) \times 10^{-3}$ [25] is 224.5 ± 9.5 events. Their ratio $R = 1.001 \pm 0.093$ is consistent with unity within the error, where 8.3% originates from the statistics of the detected $D^{*-}\ell^+\nu$ decays and 4.9% from the error on $\mathcal{B}(B^0 \to D^{*-}\ell^+\nu)$. Figure 2-b) shows the comparison of the reconstructed x^2_B distribution using the same sample to the MC simulation. The agreement between the data and MC demonstrates the validity of the present measurement.

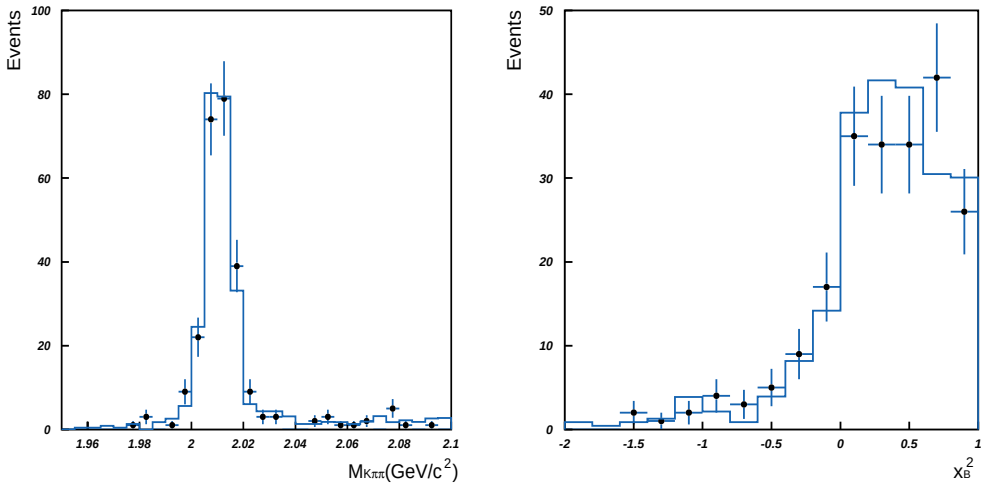

FIG. 2: Reconstructed $M(K\pi\pi)$ distribution(left) and x^2_B distribution(right) for the $D^{*-}\ell^+\nu$ calibration decay. Points with error bars are data and the histogram is the signal MC.

EXTRACTION OF BRANCHING FRACTIONS

The $B^0 \to \pi^-/\rho^-\ell^+\nu$ and $B^+ \to \pi^0/\rho^0\ell^+\nu$ signals are extracted by fitting the obtained two-dimensional distribution in (x_B^2, M_X), where M_X is the invariant mass of the X_u system. Here, the fit components are the four signal modes, the other $B^0 \to X_u^-\ell^+\nu$ and $B^+ \to X_u^0\ell^+\nu$ backgrounds and the $B\bar{B}$ background (seven components in total). The PDF (probability distribution function) for each fit component is determined from MC simulation. The $\pi/\rho\,\ell^+\nu$ signal events exhibit characteristic behavior in both of their x_B^2 and M_X distributions; other $B \to X_u\ell^+\nu$ events exhibit a weak peaking structure in x_B^2 but a broad distribution in M_X; the $B\bar{B}$ background has a relatively flat distribution in x_B^2 and a broad structure in M_X. The PDFs in (x_B^2, M_X) for each of the seven fit components are prepared for both $\bar{B}^0$ and B^- tag candidates. We then fit the two (x_B^2, M_X) distributions simultaneously, constraining contributions from the cross talk between $\bar{B}^0$ and B^- tags as well as the cross-feed between $\pi\ell^+\nu$ and $\rho\ell^+\nu$. The fitting is constrained so that the sum of the deduced branching fractions for $B \to \pi\ell^+\nu$, $B \to \rho\ell^+\nu$ and $B \to$ other $X_u\ell^+\nu$ is equal to the total inclusive branching fraction $\mathcal{B}(B \to X_u\ell\nu) = (0.25 \pm 0.06)\%$ [27].

Figure 3 presents the projections on M_X and x_B^2 of the fitting result for data in the entire q^2 region. The extracted yields for the signal components are $N(\pi^-\ell^+\nu) = 150.7 \pm 19.7$, $N(\rho^-\ell^+\nu) = 88.6 \pm 18.9$, $N(\pi^0\ell^+\nu) = 71.7 \pm 11.5$ and $N(\rho^0\ell^+\nu) = 143.3 \pm 25.4$, with the LCSR model used for the four signal PDF.

Figure 4 shows projections of the data, separated into three q^2 bins, $q^2 < 8$ GeV$^2/c^2$ and $8 \le q^2 < 16$ GeV$^2/c^2$, $q^2 \ge 16$ GeV$^2/c^2$. Here the normalization of the other $B \to X_u\ell\nu$ and the $B\bar{B}$ background components are fixed to those obtained in the above fitting for the entire q^2 region. Table I summarizes the extracted branching fractions with different FF-models for each signal mode, respectively. The results are unfolded using an efficiency matrix that relates the true and reconstructed q^2 for the three q^2 intervals. We calculate the total branching fraction by taking sum of the partial branching fractions in the three q^2 intervals.

SYSTEMATIC ERRORS

Tables II and III summarize the experimental systematic errors on the branching fractions. The experimental systematic errors can be categorized as originating from uncertainties in the signal reconstruction efficiency, the background estimation, and the normalization. The total experimental systematic error is the quadratic sum of all individual ones. We also consider the systematic error due to the dependence of the obtained branching fractions on the FF model.

The effect from the uncertainty on the signal reconstruction efficiency is evaluated based on the efficiency calibration with the $B_{sig} \to D^{*-}\ell^+\nu$ sample, discussed above. The error is taken to be that on the ratio of observed to expected number of the calibration signals (9.3%). This gives the largest contribution to the systematic error. Note this error is dominated by the statistics of the calibration signals, as explained above. Therefore, accumulation of additional integrated luminosity in the future will help to reduce this uncertainty. We further include residual errors for the reconstruction of the signal side; 1% and 2% for the detection of each charged and neutral pion, respectively, and 2% for the kaon veto and 2.1% for the lepton selection.

The systematic error due to the uncertainty on the inclusive branching fraction $\mathcal{B}(B \to$

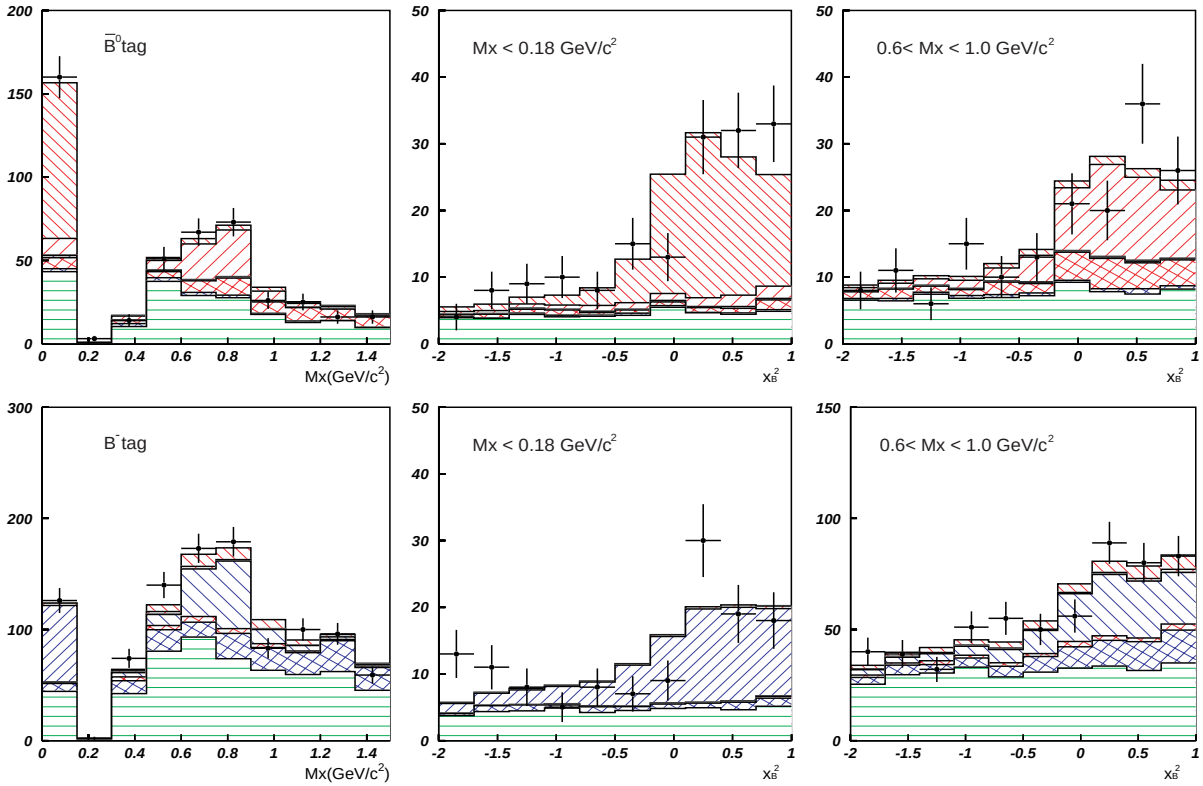

FIG. 3: Projected M_X distribution(left) and x_B^2 distributions for the mass region of π ($M_X < 0.18\text{GeV}/c^2$, middle) and ρ ($0.6 < M_X < 1.0\text{GeV}/c^2$, right) in all q^2 region; points are data. Histogram components are $\pi^-\ell^+\nu$ (red narrow 135° hatch), $\rho^-\ell^+\nu$ (red wide 45° hatch), other $X_u\ell^+\nu$ from B^0 (red cross-hatch) and $\pi^0\ell^+\nu$ (blue narrow 45° hatch), $\rho^0\ell^+\nu$ (blue wide 135° hatch), other $X_u\ell^+\nu$ from B^+ (blue cross-hatch) and $B\bar{B}$ background (green border).

$X_u\ell\nu$), which is used to constrain $X_u^-\ell^+\nu$ background, is estimated by varying this parameter within $\pm1\sigma$ of the error. The uncertainty on the $B\bar{B}$ background shape in our selection cut ($N_{\pi^+} = 1$ or $N_{\pi^+} = N_{\pi^0} = 1$ for a $\bar{B}^0$ tag and $N_{\pi^0} = 1$ or $N_{\pi^+} = N_{\pi^-} = 1$ for a B^- tag) is studied in the simulation by randomly removing charged tracks and π^0 according to the error in detection efficiency (1% for a charged track, 2% for π^0), and also by reassigning identified charged kaons as pions according to the uncertainty in the kaon identification efficiency (2%). The resultant changes in the extracted branching fractions are assigned as systematic errors. We have seen significant change for $\rho\ell^+\nu$ in the high q^2 region ($q^2 > 16$ GeV$^2/c^2$). We also vary the fraction of $B \to D^{**}\ell\nu$ decays in the $B\bar{B}$ background MC by the error quoted in [25] to test the $B \to X_c\ell\nu$ model dependence in the $B\bar{B}$ background shape. To assess the uncertainty due to the production rate of K_L^0, we vary the production rate by the error of the inclusive branching fraction of $B \to K^0\ X$ quoted in [25].

As for the normalization, we consider the uncertainty in the number of $B^0\bar{B}^0$ and B^+B^- pairs; the ratio of B^+B^- to $B^0\bar{B}^0$ pairs (f_+/f_0, 2.5%), the mixing parameter (χ_d, 1.0%) and the measured number of $B\bar{B}$ pairs ($N_{B\bar{B}}$, 1.1%).

The dependence of the extracted branching fractions on the FF model has been studied by repeating the above fitting procedure with various FF models for the signal mode and also for the cross-feed mode ($\pi\ell\nu \leftrightarrow \rho\ell\nu$). We consider the models listed in Table I. For

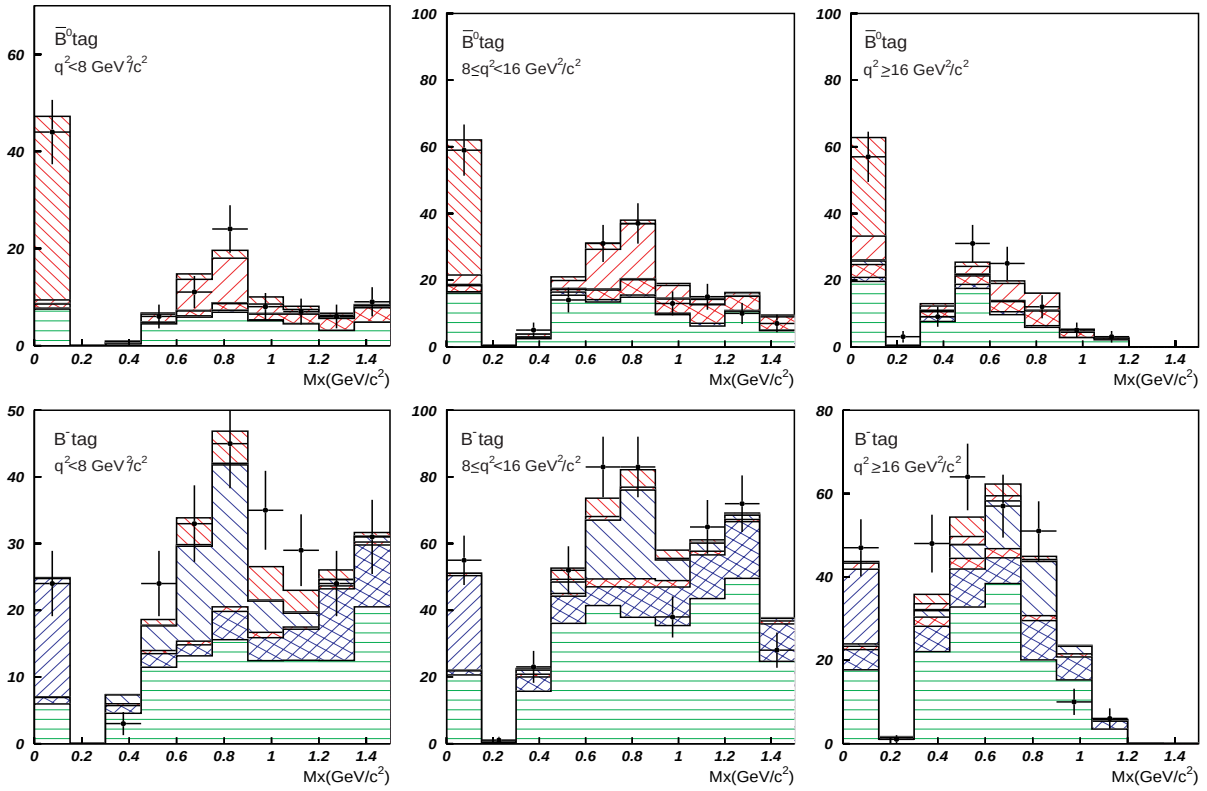

FIG. 4: Projected M_X distribution in each q^2 region; Dot is data. Histogram components are $\pi^-\ell^+\nu$ (red narrow 135° hatch), $\rho^-\ell^+\nu$ (red wide 45° hatch), other $X_u\ell^+\nu$ from B^0 (red cross-hatch) and $\pi^0\ell^+\nu$ (blue narrow 45° hatch), $\rho^0\ell^+\nu$ (blue wide 135° hatch), other $X_u\ell^+\nu$ from B^+ (blue cross-hatch) and $B\bar{B}$ background (green border).

the extracted $\mathcal{B}(B \to \pi^-(\pi^0)\ell^+\nu)$, the standard deviation among the models is $< 1.7(4.4)\%$ for $\pi\ell^+\nu$ and $< 1.9(1.4)\%$ for $\rho\ell^+\nu$. For $\mathcal{B}(B \to \rho^-(\rho^0)\ell^+\nu)$, the standard deviation is $< 6.2(1.8)\%$ for $\rho\ell^+\nu$ and $< 2.5(0.1)\%$ for $\pi\ell^+\nu$. The assigned total error due to the FF model dependence is the quadratic sum of the maximum variations with the signal and cross-feed FF models.

RESULTS

Table IV summarizes our measurements of the total and partial branching fractions for the four signal modes. Each branching fraction is obtained by taking the simple average of the values obtained from the FF models shown in Table I. The errors shown in the table are statistical, experimental systematic, and systematic due to form-factor uncertainties. The obtained branching fractions for $B^0 \to \pi^-/\rho^-\ell^+\nu$ are consistent with the existing measurements by CLEO [6] and BaBar [7, 9, 11, 13], within the measurement uncertainties. The overall uncertainty on our result for $B^0 \to \pi^-\ell^+\nu$ is 18%, comparable to that on the measurement published by CLEO [6] which is based on ν-reconstruction.

Figure 5 presents the measured q^2 distributions for each signal mode, overlaid with the best fits of FF shapes to the data. To be self-consistent, the shape of a particular FF model is

TABLE I: Extracted branching fractions for each signal mode with different FF models in units of 10^{-4}; the total branching fraction and the partial branching fractions in three q^2 intervals. χ^2/n and the probability of χ^2 shows the quality of the fit of the FF shape to the extracted q^2 distribution.

Mode	Model	$\mathcal{B}_{total}$	$\mathcal{B}_{<8}$	$\mathcal{B}_{8-16}$	$\mathcal{B}_{\geq 16}$	χ^2	$Prob.$
$\pi^-\ell^+\nu$	Ball'01	1.48 ± 0.20	0.56 ± 0.11	0.51 ± 0.11	0.41 ± 0.12	2.7/3-1	0.26
	ISGW II	1.45 ± 0.20	0.53 ± 0.11	0.53 ± 0.11	0.39 ± 0.11	4.2/3-1	0.13
	UKQCD	1.50 ± 0.20	0.55 ± 0.11	0.55 ± 0.12	0.41 ± 0.11	0.0/3-1	0.98
	Average	1.48 ± 0.20	0.55 ± 0.11	0.53 ± 0.12	0.40 ± 0.12	–	–
$\rho^-\ell^+\nu$	Ball'98	2.08 ± 0.47	0.51 ± 0.22	1.07 ± 0.29	0.49 ± 0.27	2.1/3-1	0.35
	ISGW II	2.06 ± 0.47	0.50 ± 0.20	1.00 ± 0.28	0.59 ± 0.30	0.6/3-1	0.73
	UKQCD	1.97 ± 0.44	0.48 ± 0.21	1.01 ± 0.28	0.48 ± 0.27	1.0/3-1	0.59
	Melikhov	2.20 ± 0.49	0.50 ± 0.21	1.02 ± 0.29	0.68 ± 0.34	3.3/3-1	0.19
	Average	2.07 ± 0.47	0.50 ± 0.21	1.02 ± 0.29	0.56 ± 0.30	–	–
$\pi^0\ell^+\nu$	Ball'01	0.74 ± 0.13	0.21 ± 0.06	0.32 ± 0.08	0.21 ± 0.08	2.0/3-1	0.36
	ISGW II	0.76 ± 0.13	0.20 ± 0.06	0.33 ± 0.09	0.22 ± 0.08	6.6/3-1	0.04
	UKQCD	0.80 ± 0.14	0.22 ± 0.07	0.35 ± 0.09	0.23 ± 0.08	1.1/3-1	0.58
	Average	0.76 ± 0.13	0.21 ± 0.06	0.33 ± 0.09	0.22 ± 0.08	–	–
$\rho^0\ell^+\nu$	Ball'98	1.40 ± 0.23	0.50 ± 0.12	0.57 ± 0.15	0.33 ± 0.12	1.5/3-1	0.48
	ISGW II	1.38 ± 0.23	0.48 ± 0.12	0.56 ± 0.15	0.34 ± 0.12	3.2/3-1	0.21
	UKQCD	1.36 ± 0.23	0.48 ± 0.12	0.58 ± 0.15	0.31 ± 0.12	1.4/3-1	0.49
	Melikhov	1.40 ± 0.23	0.51 ± 0.12	0.57 ± 0.15	0.32 ± 0.12	1.9/3-1	0.39
	Average	1.39 ± 0.23	0.49 ± 0.12	0.57 ± 0.15	0.32 ± 0.12	–	–

fit to the q^2 distribution extracted with the same FF model. The quality of the fit in terms of χ^2 and the probability of χ^2, shown in Table I, may provide one way to discriminate among the models. For both $B^0 \to \pi^-\ell^+\nu$ and $B^+ \to \pi^0\ell^+\nu$, the agreement with the ISGW II model is marginal, as indicated by other measurements [6, 9].

In this work, the $B^0 \to \pi^-\ell^+\nu/B^+ \to \pi^0\ell^+\nu$ and $B^0 \to \rho^-\ell^+\nu/B^+ \to \rho^0\ell^+\nu$ signals are extracted separately, which allows us to test the isospin relations. ¿From the obtained branching fractions and the B meson lifetime in [25], the ratios of decay rates are found to be,

$$\frac{\Gamma(B^0 \to \pi^-\ell^+\nu)}{\Gamma(B^+ \to \pi^0\ell^+\nu)} = (2.08 \pm 0.45 \pm 0.17), \tag{2}$$

$$\frac{\Gamma(B^0 \to \rho^-\ell^+\nu)}{\Gamma(B^+ \to \rho^0\ell^+\nu)} = (1.59 \pm 0.44 \pm 0.17), \tag{3}$$

where the first and second errors are statistical and systematic errors, respectively. The both ratios are found to be consistent with the isospin relations; $\Gamma(B^0 \to \pi^-(\rho^-)\ell^+\nu) = 2\Gamma(B^+ \to \pi^0(\rho^0)\ell^+\nu)$.

The obtained branching fractions in Table IV can be used to extract $|V_{ub}|$ using the

TABLE II: Summary of systematic errors(%) for $B^0 \to \pi^-/\rho^-\ell^+\nu$.

	$\pi^-\ell^+\nu$					$\rho^-\ell^+\nu$				
Source	$q^2<8$	$8-16$	≥ 16	<16	all	$q^2<8$	$8-16$	≥ 16	<16	all
Tracking efficiency	1	1	1	1	1	1	1	1	1	1
π^0 reconstruction	–	–	–	–	–	2	2	2	2	2
Lepton identification	2.1	2.1	2.1	2.1	2.1	2.1	2.1	2.1	2.1	2.1
Kaon identification	2	2	2	2	2	2	2	2	2	2
$D^*\ell\nu$ calibration	9.3	9.3	9.3	9.3	9.3	9.3	9.3	9.3	9.3	9.3
$Br(X_u\ell\nu)$ in the fitting	0.2	2.0	2.1	1.1	1.4	0.8	4.2	13.1	1.1	5.4
$B\bar{B}$ background shape	1.5	1.7	3.5	1.3	1.7	2.5	1.8	9.0	1.3	2.6
$Br(D^{**}\ell\nu)$	1.2	1.4	0.1	1.4	0.9	0.5	0.1	1.3	1.4	0.4
K_L^0 production rate	0.2	0.3	0.4	0.3	0.3	1.0	0.8	2.2	0.3	1.2
$N_{B\overline{B}}$	1.1	1.1	1.1	1.1	1.1	1.1	1.1	1.1	1.1	1.1
f_+/f_0	2.5	2.5	2.5	2.5	2.5	2.5	2.5	2.5	2.5	2.5
χ_d	1.1	1.1	1.1	1.1	1.1	1.1	1.1	1.1	1.1	1.1
exp. total	10.4	10.7	11.0	10.5	10.5	10.8	11.4	19.2	10.5	12.1
F.F for signal	2.6	4.0	3.1	1.9	1.7	3.3	5.4	21.4	1.9	6.2
F.F for cross-feed	2.2	3.9	5.1	2.8	1.9	2.8	2.0	6.6	2.8	2.5
F.F total	3.4	5.6	6.0	3.3	2.5	4.3	5.8	22.4	4.8	6.7

TABLE III: Summary of systematic errors(%) for $B^+ \to \pi^0/\rho^0\ell^+\nu$.

	$\pi^0\ell^+\nu$					$\rho^0\ell^+\nu$				
Source	$q^2<8$	$8-16$	≥ 16	<16	all	$q^2<8$	$8-16$	≥ 16	<16	all
Tracking efficiency	–	–	–	–	–	2	2	2	2	2
π^0 reconstruction	2	2	2	2	2	–	–	–	–	–
Lepton identification	2.1	2.1	2.1	2.1	2.1	2.1	2.1	2.1	2.1	2.1
Kaon identification	–	–	–	–	–	4	4	4	4	4
$D^*\ell\nu$ calibration	9.3	9.3	9.3	9.3	9.3	9.3	9.3	9.3	9.3	9.3
$Br(X_u\ell\nu)$ in the fitting	0.4	3.7	0.5	1.3	1.6	2.3	2.5	10.8	2.5	4.4
$B\bar{B}$ background shape	2.2	5.6	2.7	2.3	3.8	5.9	4.3	12.9	1.7	1.9
$Br(D^{**}\ell\nu)$	1.3	0.7	0.8	0.5	0.9	0.2	1.7	3.1	0.9	1.4
K_L^0 production rate	0.4	1.1	0.7	0.5	0.8	0.5	1.1	1.8	0.2	0.3
$N_{B\overline{B}}$	1.1	1.1	1.1	1.1	1.1	1.1	1.1	1.1	1.1	1.1
f_+/f_0	2.5	2.5	2.5	2.5	2.5	2.5	2.5	2.5	2.5	2.5
exp. total	10.5	12.2	10.5	10.5	11.0	12.6	12.1	20.5	11.3	12.0
F.F for signal	5.1	4.5	4.4	4.7	4.4	2.8	1.3	6.1	1.7	1.8
F.F for cross-feed	0.1	2.1	2.6	1.6	1.4	1.0	1.3	4.4	1.1	0.1
F.F total	5.1	5.0	5.1	5.0	4.6	2.9	1.8	7.5	2.0	1.8

TABLE IV: Summary of the obtained branching fractions. The errors are statistical, experimental systematic, and systematic due to form-factor uncertainties.

Modes	q^2 region (GeV$^2/c^2$)	Branching fraction ($\times 10^{-4}$)
$B^0 \to \pi^- \ell^+ \nu$	Total	$1.48 \pm 0.20 \pm 0.16 \pm 0.04$
	> 16	$0.40 \pm 0.12 \pm 0.04 \pm 0.02$
	< 16	$1.08 \pm 0.16 \pm 0.11 \pm 0.04$
$B^+ \to \pi^0 \ell^+ \nu$	Total	$0.76 \pm 0.13 \pm 0.08 \pm 0.04$
	> 16	$0.22 \pm 0.08 \pm 0.02 \pm 0.01$
	< 16	$0.54 \pm 0.11 \pm 0.06 \pm 0.03$
$B^0 \to \rho^- \ell^+ \nu$	Total	$2.07 \pm 0.47 \pm 0.25 \pm 0.14$
$B^+ \to \rho^0 \ell^+ \nu$	Total	$1.39 \pm 0.23 \pm 0.17 \pm 0.02$

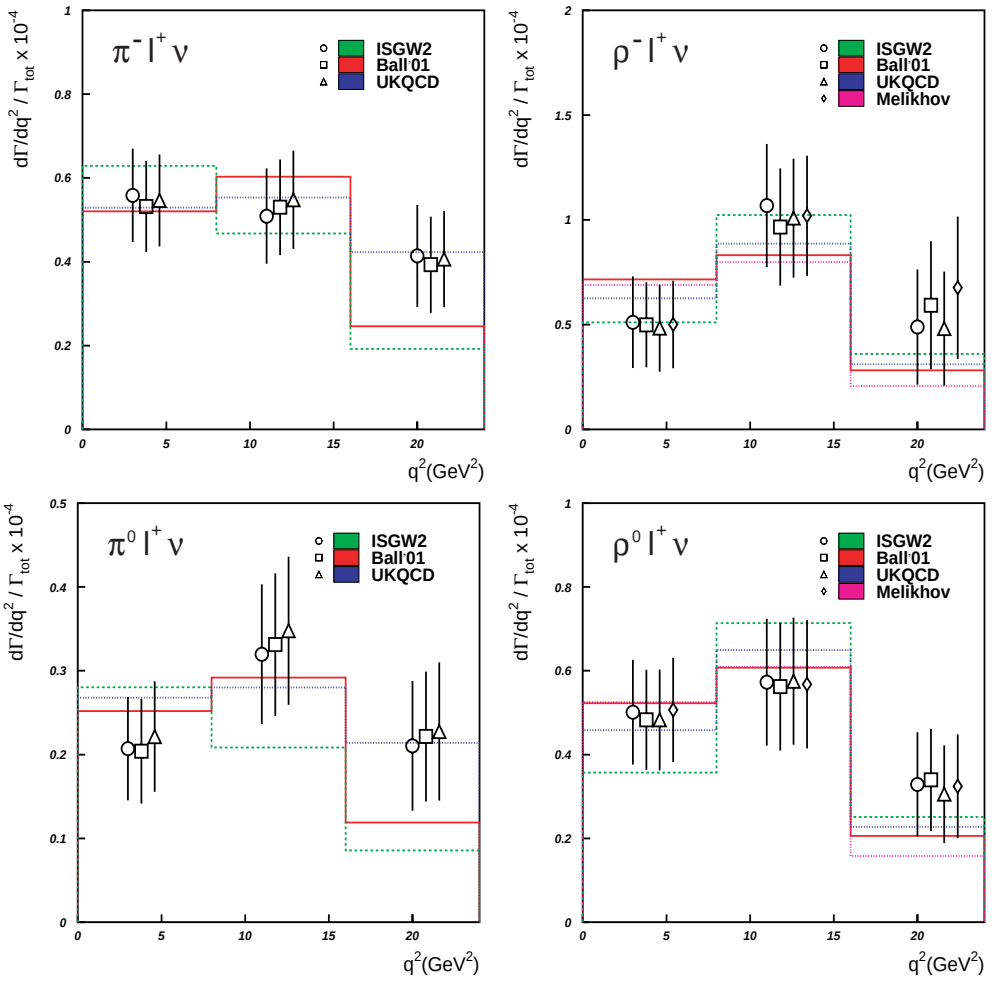

FIG. 5: Extracted q^2 distribution. Data points are shown for different FF models used to estimate the detection efficiency. Lines are for the best fit of the FF shapes to the obtained q^2 distribution.

relation,

$$|V_{ub}| = \sqrt{\frac{\mathcal{B}(B \to \pi\ell^+\nu)}{\tilde{\Gamma}_{thy}\ \tau_B}}, \tag{4}$$

where $\tilde{\Gamma}_{thy}$ is the form-factor normalization, predicted from theories. We list the partial branching fractions for $B \to \pi\ell^+\nu$ decays in the q^2 region above 16 GeV$^2/c^2$, where the LQCD calculations are the most sensitive. The table provides also the results in the region below 16 GeV$^2/c^2$, so that one can deduce $|V_{ub}|$ based on other approaches such as the LCSR calculations [28].

In this paper, we quote $|V_{ub}|$ based on the $\pi\ell^+\nu$ data in the high q^2 region and the form factor predicted by recent unquenched LQCD calculations. Their predicted $\tilde{\Gamma}_{thy}$ for the $q^2 \geq 16\,\mathrm{GeV}^2/c^2$ region are $\tilde{\Gamma}_{thy} = 1.31 \pm 0.33$ ps^{-1} (HPQCD) [2] and 1.83 ± 0.50 ps^{-1} (FNAL) [3]. We use $\tau_{B^0} = 1.532 \pm 0.009$ ps and $\tau_{B^+} = 1.638 \pm 0.011$ ps [25], and we assume the isospin relations for $\tilde{\Gamma}_{thy}$ between $B^0 \to \pi^-$ and $B^+ \to \pi^0$ transitions. Table V summarize the results, where the first and second errors are the experimental statistical and systematic errors, respectively. The third error is based on the error on $\tilde{\Gamma}_{thy}$ quoted by the LQCD authors. These theoretical errors are asymmetric because we assign them by taking the variation in $|V_{ub}|$ when $\tilde{\Gamma}_{thy}$ is varied by the quoted errors. By taking the average of the results obtained from $B^0 \to \pi^-\ell^+\nu$ and $B^+ \to \pi^0\ell^+\nu$ data, we obtain

$$|V_{ub}|^{\pi^-\ell^+\nu+\pi^0\ell^+\nu}_{(q^2\geq 16)} = (4.50 \pm 0.52 \pm 0.27^{+0.70}_{-0.48}) \times 10^{-3}(\mathrm{HPQCD}), \tag{5}$$

$$|V_{ub}|^{\pi^-\ell^+\nu+\pi^0\ell^+\nu}_{(q^2\geq 16)} = (3.81 \pm 0.44 \pm 0.23^{+0.66}_{-0.43}) \times 10^{-3}(\mathrm{FNAL}). \tag{6}$$

TABLE V: Summary of $|V_{ub}|$ obtained from the $B \to \pi\ell^+\nu$ data in the $q^2 > 16\,\mathrm{GeV}^2/c^2$ region. The first and second errors are experimental statistical and systematic errors, respectively. The third error stems from the error on $\tilde{\Gamma}_{thy}$ quoted by the LQCD authors.

Theory	$\tilde{\Gamma}_{thy}$(ps^{-1})	Mode	$\lvert V_{ub}\rvert(\times 10^{-3})$
HPQCD	1.31 ± 0.33	$\pi^-\ell^+\nu$	$4.49 \pm 0.65 \pm 0.28^{+0.70}_{-0.48}$
		$\pi^0\ell^+\nu$	$4.53 \pm 0.81 \pm 0.26^{+0.71}_{-0.48}$
		$\pi^-\ell^+\nu + \pi^0\ell^+\nu$	$4.50 \pm 0.52 \pm 0.27^{+0.70}_{-0.48}$
FNAL	1.83 ± 0.50	$\pi^-\ell^+\nu$	$3.80 \pm 0.55 \pm 0.24^{+0.66}_{-0.43}$
		$\pi^0\ell^+\nu$	$3.83 \pm 0.69 \pm 0.22^{+0.66}_{-0.44}$
		$\pi^-\ell^+\nu + \pi^0\ell^+\nu$	$3.81 \pm 0.44 \pm 0.23^{+0.66}_{-0.43}$

These values are in agreement with those from the inclusive $B \to X_u\ell\nu$ decays [29]. The experimental precision in the above $|V_{ub}|$ determination is 13%, and it is currently dominated by the statistical error of 12%. By accumulating more luminosity, a measurement with errors below 10% is feasible. With improvement in unquenched LQCD calculations, the present measurement will provide a more accurate determination of $|V_{ub}|$.

We thank the KEKB group for the excellent operation of the accelerator, the KEK Cryogenics group for the efficient operation of the solenoid, and the KEK computer group

and the National Institute of Informatics for valuable computing and Super-SINET network support. We acknowledge support from the Ministry of Education, Culture, Sports, Science, and Technology of Japan and the Japan Society for the Promotion of Science; the Australian Research Council and the Australian Department of Education, Science and Training; the National Science Foundation of China under contract No. 10175071; the Department of Science and Technology of India; the BK21 program of the Ministry of Education of Korea and the CHEP SRC program of the Korea Science and Engineering Foundation; the Polish State Committee for Scientific Research under contract No. 2P03B 01324; the Ministry of Science and Technology of the Russian Federation; the Ministry of Education, Science and Sport of the Republic of Slovenia; the National Science Council and the Ministry of Education of Taiwan; and the U.S. Department of Energy.

[1] M. Kobayashi and T. Maskawa, Prog. Theor. Phys. **49**, 652 (1973).
[2] J. Shigemitsu *et al.*, hep-lat/0408019 (Contribution to Lattice, Batavia, IL, 2004).
[3] M. Okamoto *et al.*, hep-lat/0409116 (Contribution to Lattice, Batavia, IL, 2004).
[4] J. P. Alexander *et al.* (CLEO Collaboration), Phys. Rev. Lett. **77**, 5000 (1996).
[5] J. P. Alexander *et al.* (CLEO Collaboration), Phys. Rev. **D61**, 052001 (2000).
[6] S. B. Athar *et al.* (CLEO Collaboration), Phys. Rev. **D 68**, 072003 (2003).
[7] B. Aubert *et al.* (BaBar Collaboration), Phys. Rev. Lett. **90**, 181801 (2003).
[8] K. Abe *et al.* (Belle Collaboration), Phys. Rev. Lett. **93**, 131803 (2004).
[9] B. Aubert *et al.* (BaBar Collaboration), hep-ex/0507003.
[10] K. Abe *et al.* (Belle Collaboration), hep-ex/0408145 (Contribution to ICHEP2004, Beijing, August 16-22, 2004).
[11] B. Aubert *et al.* (BaBar Collaboration), hep-ex/0506064 (Contribution to Lepton-Photon 05, Uppsala, June 30 - July 5, 2005).
[12] B. Aubert *et al.* (BaBar Collaboration), hep-ex/0506065 (Contribution to Lepton-Photon 05, Uppsala, June 30 - July 5, 2005).
[13] B. Aubert *et al.* (BaBar Collaboration), hep-ex/0408068 (Contribution to ICHEP 2004, Beijing, August 16-22, 2005).
[14] S. Kurokawa and E. Kikutani, Nucl. Instr. and Meth. A **499**, 1 (2003), and other papers included in this volume.
[15] A. Abashian *et al.* (Belle Collaboration), Nucl. Instr. and Meth. A **479**, 117 (2002).
[16] Y. Ushiroda (Belle SVD2 Group), Nucl. Instr. and Meth.A **511** 6 (2003).
[17] R. Brun *et al.*, GEANT3.21, CERN Report DD/EE/84-1 (1984).
[18] D. Scora and N. Isgur, Phys. Rev. D **52**, 2783 (1995).
[19] P. Ball and R. Zwicky, JHEP **0110**, 019 (2001).
[20] P. Ball and V. M. Braun, Phys. Rev. D **58**, 094016 (1998).
[21] L. Del Debbio, J. M. Flynn, L. Lellouch, and J. Nieves (UKQCD Collaboration), Phys. Lett. B **416**, 392 (1998).
[22] D. Melikhov, Phys. Rev. D **53**, 2460 (1996).
[23] F. De Fazio and M. Neubert, JHEP **9906**, 017 (1999).
[24] Evtgen event generator, http://hep.ucsb.edu/people/lange/EvtGen/.
[25] Particle Data Group, http://pdg.lbl.gov/, 2005.
[26] Heavy Flavor Averageing Group, LP2003

[27] H. Kakuno *et al.* (Belle Collaboration), Phys. Rev. Lett **92**, 071802 (2004); the inclusive branching fraction used in the fitting is based on the partial branching fraction $\Delta\mathcal{B}(B \to X_u \ell\nu; M_X < 1.7\mathrm{GeV}/c^2, q^2 > 8\ \mathrm{GeV}^2/c^2)$ and a calculation of f_u shown in hep-ex/0408115.
[28] P.Ball and R.Zwicky, Phys. Rev. D **71**, 014015 (2005).
[29] Heavy Flavor Averaging Group, "Updates of Semileptonic Results for EPS 2005", http://www.slac.stanford.edu/xorg/hfag/semi/eps05/eps05.shtml.